Role of Intrasurface Hydrogen Bonding on Silica Dissolution

Shikha Nangia and Barbara J. Garrison*

104 Chemistry Building, Department of Chemistry, The Pennsylvania State University, University Park, Pennsylvania 16802

Received: October 14, 2009; Revised Manuscript Received: November 24, 2009

A recently formulated reactive Monte Carlo (RxMC) algorithm has been applied to determine the differential dissolution probability in topographically distinct crystallographic faces of β-cristobalite. Although the contribution of edge, kink, and step sites to the overall dissolution from a crystal is well-established, the effect of hydrogen bonding on flat terrace sites is less understood. In an earlier study (*J. Phys. Chem.* **111**, *5169*, 2007), 40 β-cristobalite surfaces were shown to have distinct intrasurface hydrogen bonding patterns between the hydroxylated surface groups. This study is an extension of the previous work with the aim to identify the role intrasurface hydrogen bonding has toward overall dissolution from these surfaces. Five surfaces have been chosen with varying ratios of Q^2 (two surface OH groups per Si site) and Q^3 (one surface OH group per Si site) groups. The results successfully show that pure Q^2 {100} terrace sites with intrasurface hydrogen are less reactive than non-hydrogen bonded pure Q^3 {111} terrace sites. The newly formulated RxMC algorithm for silica−water dissolution highlights the unique features of the terrace sites and distinguishes one surface from the other.

Introduction

Interfaces provide a confluence of physical and chemical interactions between distinct phases. Interfacial interactions play a big role in aerosols, transport through biological membranes, corrosion of metals, and dissolution of rocks.[1−7] Each situation has unique interfacial characteristics, but the interaction of water with ordered solid surfaces is particularly fascinating because of strong hydrogen bonding characteristics that can lead to tessellation if the surface geometry matches.[8−10] Tessellation of water occurs when water overlayers form an icelike ordered arrangement through hydrogen bonds among themselves and the dangling groups of the solid, although hydrophilicity of the surface is crucial for water tessellation but hydrophilicity alone is not sufficient to form ordered water overlayers. Both experimental and computational studies show that tessellation varies, depending on the topography and separation between neighboring groups.[1−17] The neighboring surface groups can also form intrasurface hydrogen bonding among themselves.[8,10] Even though water tessellation and intrasurface bonding combined can lead to stable intricate networks, it is not clear what effect they have on the chemical reactivity of a surface.

Experimentally, water overlayers on solids have been studied using modified atomic force microscopy to obtain nanometer resolution images of water following the epitaxy of the underlying surface.[11] To focus on the OH bonds involved in the hydrogen bonding at the interface, the most popular method is the sum-frequency vibrational spectroscopy (SFVS).[12−20] Using the SFVS technique, Ostroverkhov et al. showed vibrational spectra with ice peaks of water tessellated on the (0001) plane of α-quartz.[15] In a follow-up study, Ostroverkhov et al. proposed that the icelike interface persists with the change in pH, but water molecules tend to change their orientation.[16] In another study, Schlegel et al.[21] showed that the height of the water overlayers was face-specific, based on the surface silanol groups. Despite the experimental data proving the existence of icelike patterns of water on specific crystallographic planes of silicate minerals, none of these techniques reveal how the tessellation of one surface differs from the other. Does the chemical reactivity and dissolution depend on the stability of tessellation? If tessellation affects dissolution, then different surfaces can contribute differently to the overall dissolution.

Tessellation and intrasurface hydrogen bonded networks have also been observed for hydroxylated silicate surfaces using computational methods.[8−10,22,23] Yang et al. used ab initio density functional calculations on β-cristobalite,[8] a silicate mineral and polymorph of quartz. The β-cristobalite crystal has tetrahedral SiO_4^{4-} units, and depending on the number of bridged Si−O−Si bonds, each Si is labeled Q^i. The calculations by Yang et al. revealed that hydroxylated (100) β-cristobalite surface, composed of exclusively Q^2 sites (2 OH groups per Si surface site) exhibits tessellation in the presence of water, but in the absence of water, it is capable of forming a network of intrasurface hydrogen bonds.[8]

The role of intrasurface hydrogen bonding and tessellation is not explicitly included in face-specific dissolution kinetics models.[24−32] The focus of these kinetic models is to compute an overall dissolution rate controlled by reactive surface features such as kinks, edges, steps, defects, etch-pits, and development of reactive surface area. The kinetic Monte Carlo models have been successfully applied to several class of minerals; for example, carbonates,[29] silicates,[30] and aluminosilicates.[32] It is, however, important to identify how dissolution from topographically flat terrace sites of various crystallographic faces compare with each other in a thermodynamically controlled process.

In an alternative modeling approach, Du and de Leeuw performed molecular dynamics (MD) simulations of modeling dissolution of (0001) α-quartz surface in water and found that ordered overlayers existed on the quartz surface, and the extent of dissolution was limited.[26] They suggested that complete dissolution of the quartz surface is unlikely due to entropic factors, and for the limited successful dissolution events, the leaving $Si(OH)_4$ species remained close to the surface. This

* Corresponding author. E-mail: bjg@psu.edu.

10.1021/jp909878b
Published on Web 12/29/2009

observation, however, could be a limitation of the MD method in which these simulations were carried out for about 100 ps. It is likely that the migration of the $Si(OH)_4$ species would be observed if the MD simulations are run for a longer time.

Previously, our detailed study of 40 hydroxylated β-cristobalite surfaces showed that with the exception of the (100) plane, the remaining surfaces have less stable intrasurface hydrogen bonding and weaker tessellation.[10] The analysis showed that all studied β-cristobalite surfaces have varying ratios of Q^2 and Q^3 surface sites; the details have been presented elsewhere.[10] The conclusion of the study was that for β-cristobalite surfaces, there were three main aspects that controlled the tessellation: (a) separation between neighboring OH surface sites, (b) surfaces with higher Q^2:Q^3 ratios formed hydrogen bonded motifs more readily, and (c) flatness of the surface. The aforementioned computational studies provide evidence of variations in physical interactions of various β-cristobalite surfaces, and therefore, it is logical to extend this study to understand the contribution of the variations in chemical interactions and dissolution.

A newly formulated Monte Carlo (MC) method circumvents these limitations of MD techniques and utilizes the advanced reactive[33−39] (RxMC) and configurational bias (CBMC) Monte Carlo techniques.[40] The combined RxMC−CBMC algorithm was developed for silica dissolution/precipitation reactions and has been reported previously.[40] This algorithm is a time-independent methodology that alleviates the limitation of running expensive MD simulations for extended times to observe significant chemical events. Instead, the new algorithm uses stochastic positional moves to provide the ensemble-averaging of the system. The theoretical development of the RxMC−CBMC algorithm is key to the application in the present article. The aim is to apply the new RxMC−CBMC algorithm to calculate the differential contribution to the overall dissolution for β-cristobalite surfaces due to tessellation and intrasurface hydrogen bonding.

The remaining article has been subdivided into sections. In Section I, an overview of the reactive MC and configurations is provided. Section II describes the system setup and the β-cristobalite surfaces that were chosen for this study. The results and discussions are presented in Section III. Finally, the conclusions are provided in Section IV.

I. Methodolgy: RxMC−CBMC Algorithm

Our method of determining the differential dissolution of β-cristobalite surfaces is the combined RxMC and CBMC algorithm. Unlike the conventional MC applications of finding a lower energy configuration in different phases, the RxMC method provides an elegant formulation to use the MC technique on systems undergoing bond-breaking and bond-making processes. The RxMC formulation allows the chemical species in the system to change their identity; that is, to change from reactants to products and vice versa. More specifically, for a reaction

$$\nu_1 M_1 + \nu_2 M_2 \leftrightarrow \nu_3 M_3 + \nu_4 M_4 \tag{1}$$

with ν_i being stoichiometry coefficients for M_i chemical species, the total number of atoms are conserved. At equilibrium, the total chemical potential μ_i for the system is zero. In general, the probability of a C-component system to exist in any configuration α is

$$P_\alpha = \frac{1}{\Xi} e^{-U_\alpha/k_B T}\left\{ e^{1/k_B T \sum_{i=1}^{C} N_i^\alpha \mu_i} \prod_{i=1}^{C} \frac{q_i^{N_i^\alpha}}{N_i^\alpha!} \right\} \tag{2}$$

where Ξ is the grand canonical partition function; U_α is the potential energy; T is the temperature; k_B is the Boltzmann constant; and for the ith component, N_i and q_i are the number of molecules and partition function, respectively. Using the P_α for configuration, $\alpha = r$ for the reactant, $\alpha = p$ for the reactant and product configuration, the transition probability of forming the product from reactants is given by

$$P(p \leftrightarrow r) = e^{-(U_p - U_r)/k_B T} \prod_{i=1}^{C} \frac{N_i!}{(N_i + \nu_i)!} \prod_{i=1}^{C} q_i^{\nu_i} \tag{3}$$

where the terms containing the canonical partition function and chemical potential drop out of the transition probability. To accept a move, the transition probability is compared to a random number in the Monte Carlo scheme.

The above algorithm was combined with the CBMC scheme described earlier.[40] This addition was done to improve the efficiency of the algorithm to sample systems with disparately sized components. For example, in the hydrolysis reaction

$$Q^4 - O - Q^1(s) + H_2O(l) \leftrightarrow Q^3 - OH(s) + Q^0(aq) \tag{4}$$

the Q^1 surface group is removed and a Q^0 group is inserted in solution. The volume size ratio of silicic acid is 4: 1 implying that the insertion of Q^0 in solution will result in overlapping with approximately four water molecules. In most cases, a simulation with this size disparity is highly inefficient because most of the dissolution attempts will fail due to high-energy overlapping configurations in the system. An algorithmic improvement for this situation is to choose moves in which the water molecules overlapping the Q^0 are removed and then using the Rosenbluth weighting factor[41−46] reinserted back into bulk water. The enhancement of the RxMC method with the CBMC scheme is specifically important for the present application.

II. System Setup

The simulation setup for these calculations started with generating crystallographic planes of β-cristobalite using a surface generation module in Cerius^2 software.[47] β-Cristobalite has a cubic face-centered lattice with a $Fd3m$ space group. The unit cell dimensions are $a = b = c = 7.16$ Å and $\alpha = \beta = \gamma = 90°$. Since the unit cell is symmetric along all three axes, it makes the crystallographic planes (100), (010), and (001) equivalent, and thus, the entire family of these equivalent planes will be written as {100}.

In all, five crystallographic planes—namely, {100}, {011}, {013}, {011}, and {111}—are presented here. The slab dimensions for the simulation cell are reported in Table 1. The cleaved surfaces with unhydroxylated Si−O bonds and under-coordinated Si atoms in the $x-y$ plane were capped with H or OH groups, respectively, to hydroxylate the entire surface. The top $x-y$ plane of β-cristobalite was exposed to a box of water with dimensions of the surface and column height of 100 Å. The bottom $x-y$ plane of β-cristobalite was held fixed to mimic an infinitely deep sample. Along the $x-z$ and $y-z$ planes, periodic

TABLE 1: Cell dimensions (in Å) of the simulation box

surface	length	breadth	depth
100	45	45	16
111	92	42	14
011	58	42	11
013	59	37	13
113	61	32	13

TABLE 2: Percentages of Si Surface Sites for the Five β-Cristobalite Surfaces and the Distances (Å) between Neighboring Surface Sites

	site percentages		distances	
surfaces	Q^2	Q^3	intra O−O	inter O−H
{011}	0	100	4.8	
{111}	0	100	5.2	
{113}	25	75	3.1	2.2
{013}	50	50	3.0	2.2
{100}	100	0	2.7	2.1

boundary conditions were applied to the entire system, including the box of water.

These surfaces were chosen on the basis of the surface constitution of Q^2 and Q^3 sites and are reported in Table 2. From among all these planes, the {100} surfaces have exclusively Q^2 sites, which makes them strikingly dissimilar to {011} and {111} surfaces, both of which have exclusively Q^3 sites. On the other hand, the {013} and {113} planes have both Q^2 and Q^3 sites in ratios indicated in Table 2. It has been reported earlier that the intrasurface hydrogen bonding depends on the fraction of Q^2 sites; however, it is not clear how the physical interactions can affect the contribution to chemical dissolution from these characteristically dissimilar surfaces.

The silica-water interactions are described by the potential energy function proposed by Fueston and Garofalini.[48] The functional form accounts for interactions between the two closest neighbors and three bonded neighbors within a 5.5 Å cutoff radius.[49,50] The functional form and parameters used have been provided elsewhere and are therefore not repeated here.[48,51−56]

III. Results and Discussion

The simulation for hydrolyzing Si−O−Si bonds of the surface reactive site was performed using the stepwise dissolution algorithm that provided reasonable agreement with the experimental dissolution data in a previous study.[40] In each dissolution step, one water molecule is consumed per Si−O−Si bond hydrolyzed, resulting in a more hydroxylated Si site; for example, $Q^3 \leftrightarrow Q^2$, $Q^2 \leftrightarrow Q^1$, or $Q^1 \leftrightarrow Q^0$. The reverse reactions of hydrolyzed Q^0 groups reacting with the surface in a precipitation reaction are sampled along with the possible polymerization events in solution. Before looking at the dissolution trends and interpreting the data, it is essential to highlight the surface topography before and after a stepwise hydrolysis reaction. From among the surfaces studied here, the {100} and {111} surfaces are described in detail because of their structurally distinct characteristics. The {110} surface is pure Q^3 just like the {111} surface, and the remaining two surfaces have intermediate topologies. Pictorial depictions of the surfaces have been presented earlier.[10]

The {100} surface is shown in Figure 1 without any water overlayers. This surface is extensively hydrogen bonded, with both of the Q^2 hydroxyl groups bonded to their closest neighbors. In addition, the Q^2 Si atomic layer is bonded to the underlying Q^4 Si layer through bridging O atoms. To hydrolyze the Si(Q^2)−O−Si(Q^4) bond, the water molecule has to penetrate

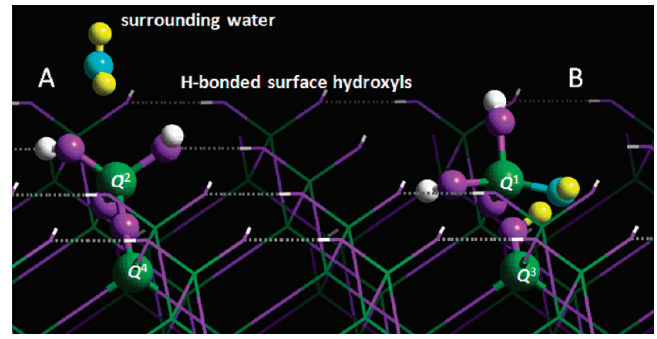

Figure 1. The {100} β-cristobalite surface with (A) initial intrasurface hydrogen bonding pattern and (B) disrupted hydrogen bonding pattern after the dissolution step is shown. The snapshot has Si (green), O (purple), and H (white) atoms and intrasurface hydrogen bonds (gray). Only a single surrounding water molecule is shown for clarity with O (blue) and H (yellow) atoms.

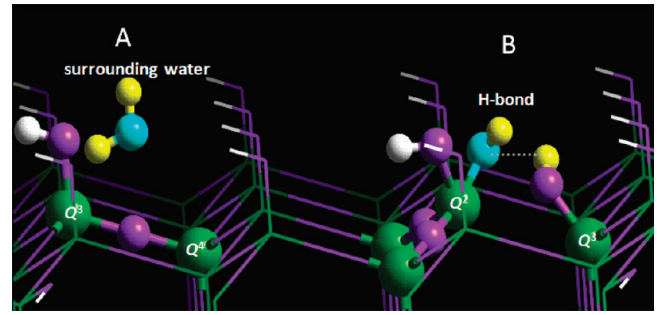

Figure 2. A snapshot of the {111} β-cristobalite surface is shown (A) lacking intrasurface hydrogen bonding before the dissolution and (B) some hydrogen bonding after dissolution. The color scheme is the same as in Figure 1.

the stable hydrogen bonded surface network, as shown in Figure 1A. Moreover, one of the H atoms from the water molecule must attach to the bridging O atom, which has steric hindrance for changing its local geometry. A consequence of this first step toward dissolution is that the continuity of the hydrogen-bonded network is destroyed, as shown in Figure 1B. Although Figure 1 does not show the water overlayers on the {100} surface, these overlayers tessellate and further prevent the dissolution process.

Conversely, the {111} surface does not have a hydrogen bonded network with the neighboring sites. In the presence of water, however, the surface can form linear hydrogen bonded chains with the water overlayer. For the ease of depiction, a {111} surface without the water overlayer is shown both before and after the first hydrolysis step in Figure 2. The separation between neighboring Q^3 sites is large, as shown by the O−O separation in Table 2, thus indicating a lack of a hydrogen bond networks.[10] The hydrolyzing water molecule, therefore, has easier access to the Si(Q^3)−O−Si(Q^4) bridge bond. Once hydrolyzed, however, the newly formed Q^2 and Q^3 sites form hydrogen bonds that stabilize the product configuration.

The measure we have chosen to use for the extent of dissolution is the number of Q^0 groups in solution divided by the Si number of sites on the initial pristine surface. This normalization with respect to the number of initial surface sites makes the results independent of the depth of the sample. Figure 3 shows the normalized dissolution extent, Si (aq)/Si (initial surface) for the entire length of the simulation until all five systems reach equilibrium. The systems reach equilibrium when the forward reaction of surface dissolution becomes equal to the back reaction of precipitation. As pointed out previously,[40]

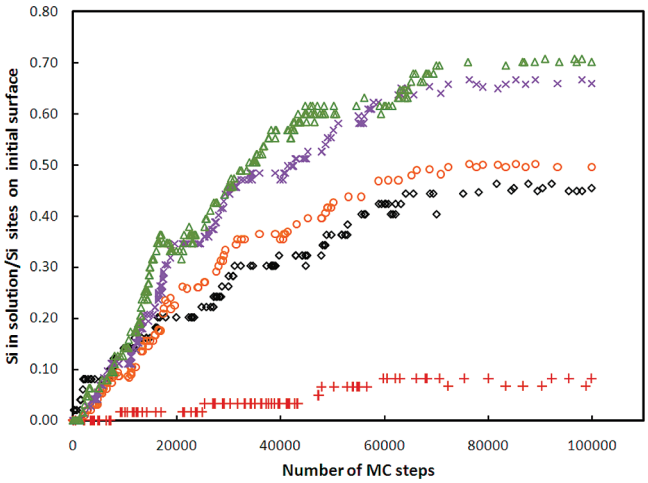

Figure 3. Comparison of dissolution trends in plot of the ratio of the number of Si's in solution to the number of Si sites in the initial surface versus number of MC moves for {100} (plus, red), {013} (diamond, black), {113} (circle, orange), {111} (triangle, green), and {110} (cross, purple).

TABLE 3: Q^i Site Data for the Initial and Equilibrated {100} and {111} Surfaces

	{100} surface		{111} surface	
Si sites	initial	equilibrated	initial	equilibrated
Q^4	968	959	1152	1124
Q^3	0	7	144	32
Q^2	121	110	0	19
Q^1	0	4	0	20
Q^0	0	9	0	101

the amount of silicic acid in solution is controlled by the surface topology. The dissolution for the {111} surface is highest with the equivalent of 70% of the top Si layer removed, closely followed by the {011} surface with 68%. The similarity in dissolution trends for both the {011} and {111} surfaces indicates that the pure Q^3 surfaces have similar dissolution mechanisms and physical surface interactions. The dissolution extents of the {111} and {011} surfaces are about 7−8 times higher than the {100} surface. This implies that although complete dissolution of a Si site on {011} and {111} surfaces requires hydrolysis of three Si−O−Si bonds, but because of lack of any physical interactions between the surface groups, the dissolution is high. The extensive hydrogen-bonding on the {100} surface renders it less reactive to dissolution. The remaining two surfaces, {013} and {113}, have dissolution extents in the 40−50% range, intermediate between the pure Q^2 and Q^3 surfaces. The intermediate dissolution extents appear to be a consequence of the mixed Q^2 and Q^3 surface compositions, which seem to partially inherit the {111} and {100} attributes.

To highlight the differences in the {100} and {111} surfaces, we will focus on the solid phase evolution of the Si sites in the MC simulation. In Table 3, the number of Q^i sites in the {100} and {111} surfaces is provided in the initial and equilibrated system. The {100} surface initially has 121 Q^2 sites and 968 Q^4 sites. After equilibrium is obtained, this balance shifts slightly, because only nine Q^0 are released to solution, leaving few Q^1 and Q^3 surface sites behind. The removal of the nine Q^0 occurs only from the top two Si layers of the solid, as shown in Figure 4. The top layer has six vacancies in Figure 4B, and the second layer has three vacancies (Figure 4D), two of which are directly below the vacancies in the top layer. There is one

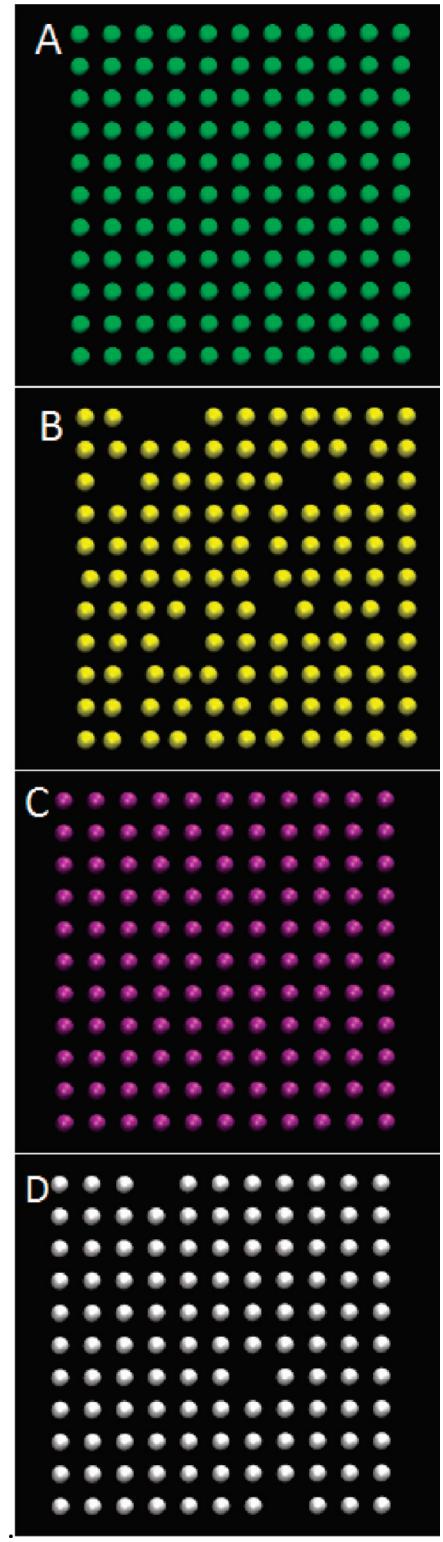

Figure 4. Cross-sectional view of the {100} cristobalite surface showing only the Si: (A) Top layer, before (green); (B) top layer, after (yellow); (C) second layer, before (purple); and (D) second layer, after (white). The atomic positions of O and H atoms are not shown for clarity.

vacancy in the lower right corner of the second layer with no vacancy in the first layer above it. The simulation allows for the $Q^1 \leftrightarrow Q^2$ back reaction; thus, a second-layer vacancy can get covered. Another indication of the back reaction is the slight disarray in the top Si layer of the equilibrated surface shown in Figure 4C.

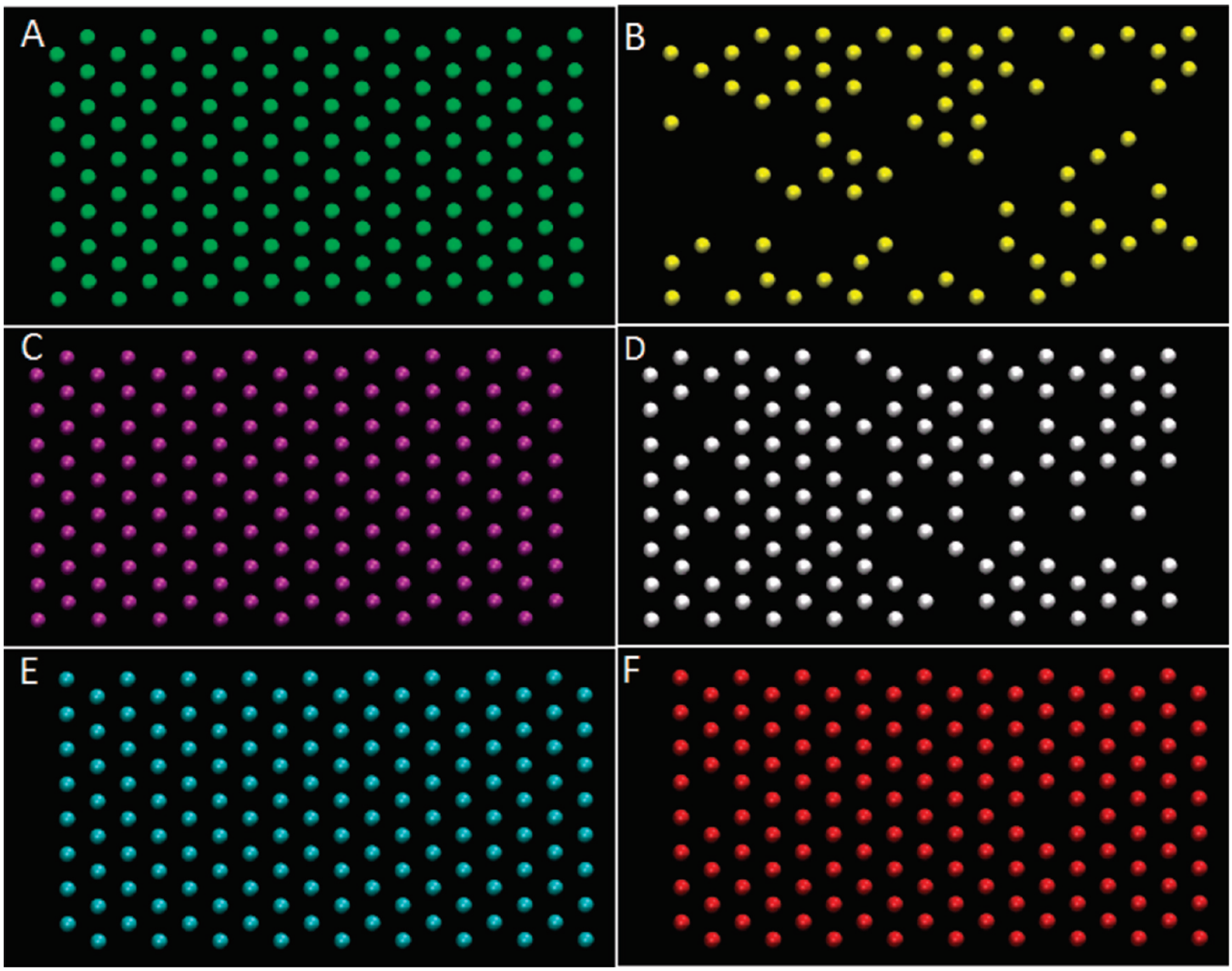

Figure 5. Cross-sectional view of the {111} cristobalite surface showing only the Si atoms. (A) Top layer, before (green); (B) top layer, after (yellow); (C) second layer, before (purple); (D) second layer, after (white); (E) third layer, before (blue), and (F) third layer, after (red). The atomic positions of O and H atoms are not shown for clarity.

A similar analysis of the Q^i sites of the {111} surface shows 144 Q^3 sites initially, but with 70% equivalent of the top layer dissolved, only 32 Q^3 sites remain, as given in Table 3. The number of silicic acid molecules (Q^0) in solution is a factor of 10 higher than the {100} system. The vacancies created by dissolution in the top three layers are shown in Figure 5. The top layer lost 70% of the Si sites; the second layer, about 20%; and the third layer, <1%. The {111} surface undergoes the stepwise $Q^3 \leftrightarrow Q^2 \leftrightarrow Q^1$ dissolution with minimal back reaction. The hydrolysis continues through the second and third Si layers. The equilibrated {111} is much rougher as compared to the {100} surface.

The results on all five surfaces consistently show that differences in surface topology, especially with respect to intrasurface hydrogen bonding, have significant differences in chemical reactivity. Each of these reactions on the surfaces results in the hydrolysis or formation of a Si−O−Si bond, but the probability of the reaction is influenced by factors that are typically considered less significant than the barrier heights for the chemical reactions. The collective physical interactions of surface sites lead to differential dissolution trends that are unique to each surface.

IV. Conclusions

Intrasurface hydrogen bonding and water tessellation have been shown to exist by both experimental and computational techniques. The present study conclusively demonstrates that hydrogen bonding causes differential dissolution reactivity on the terrace sites of β-cristobalite surfaces. The most significant comparison is between the pure Q^2 and pure Q^3 surfaces. In principle, the fewer number of bonds to be broken for complete removal of the reactive group from the surface, the easier the dissolution. Therefore, the hydrolysis at a pure Q^2 terrace site is expected to occur more readily because two Si−O−Si bonds need to be hydrolyzed, as compared to three for a Q^3 terrace site. Contradictory to the expected trend, the dissolution probability for a pure Q^2 terrace site is much less due to extensive stabilization by intrasurface hydrogen bonding and tessellation. The $Q^2 \leftrightarrow Q^1$ dissolution reactions do occur, but because of the proximity of the neighboring sites, the back reactions also occur readily, preventing the removal of Si from the surface. The networking between the dangling bonds tends to passivate the reactivity of the terrace sites. This result suggests that chemical reactivity of terrace sites does not exclusively depend on the reactive sites; rather, it depends on how the

surface groups interact with each other and with their immediate surroundings.

Additionally, this study highlights the success of designing a combined RxMC−CBMC approach for reactive systems that are computationally affordable. The method combines stochastic sampling of the MC method to simulate all reaction combinations that occur at the solid−liquid interface. So far, the algorithm has been applied to silicates, but it has the potential to be extended to more complicated and intensive systems.

Acknowledgment. This work has been supported by the National Science Foundation NSF under Grant no. CHE-0535656.

References and Notes

(1) Nagy, K. L. *Chemical Weathering Rates of Silicate Minerals* **1995**, *31*, 173.
(2) Brown, G. E.; Foster, A. L.; Ostergren, J. D. *Proc. Natl. Acad. Sci. U.S.A.* **1999**, *96*, 3388.
(3) Buck, R. P.; Lindner, E. *Acc. Chem. Res.* **1998**, *31*, 257.
(4) Barker, W. W.; Banfield, J. F. *Geomicrobiol. J.* **1998**, *15*, 223.
(5) Feller, S. E. *Curr. Opin. Colloid Interface Sci.* **2000**, *5*, 217.
(6) Tian, Z. Q.; Ren, B. *Annu. Rev. Phys. Chem.* **2004**, *55*, 197.
(7) Zhang, R.; Somasundaran, P. *Adv. Colloid Interface Sci.* **2006**, *123*, 213.
(8) Yang, J.; Meng, S.; Xu, L. F.; Wang, E. G. *Phys. Rev. Lett.* **2004**, *92*, 146102.
(9) Yang, J.; Wang, E. G. *Phys. Rev. B* **2006**, *73*, 035406.
(10) Nangia, S.; Washton, N. M.; Mueller, K. T.; Kubicki, J. D.; Garrison, B. J. *J. Phys. Chem. C* **2007**, *111*, 5169.
(11) Hu, J.; Xiao, X. D.; Ogletree, D. F.; Salmeron, M. *Science* **1995**, *268*, 267.
(12) Du, Q.; Freysz, E.; Shen, Y. R. *Phys. Rev. Lett.* **1994**, *72*, 238.
(13) Du, Q.; Freysz, E.; Shen, Y. R. *Science* **1994**, *264*, 826.
(14) Miranda, P. B.; Shen, Y. R. *J. Phys. Chem. B* **1999**, *103*, 3292.
(15) Ostroverkhov, V.; Waychunas, G. A.; Shen, Y. R. *Chem. Phys. Lett.* **2004**, *386*, 144.
(16) Ostroverkhov, V.; Waychunas, G. A.; Shen, Y. R. *Phys. Rev. Lett.* **2005**, 94.
(17) McGuire, J. A.; Shen, Y. R. *Science* **2006**, *313*, 1945.
(18) Shen, Y. R.; Ostroverkhov, V. *Chem. Rev.* **2006**, *106*, 1140.
(19) Ji, N.; Ostroverkhov, V.; Chen, C. Y.; Shen, Y. R. *J. Am. Chem. Soc.* **2007**, *129*, 10056.
(20) Ji, N.; Ostroverkhov, V.; Tian, C. S.; Shen, Y. R. *Phys. Rev. Lett.* **2008**, 100.
(21) Schlegel, M. L.; Nagy, K. L.; Fenter, P.; Sturchio, N. C. *Geochim. Cosmochim. Acta* **2002**, *66*, 3037.
(22) Yang, J. J.; Meng, S.; Xu, L. F.; Wang, E. G. *Phys. Rev. B* **2005**, 71.
(23) Goumans, T. P. M.; Wander, A.; Brown, W. A.; Catlow, C. R. A. *Phys. Chem. Chem. Phys.* **2007**, *9*, 2146.
(24) Lasaga, A. C.; Luttge, A. *Science* **2001**, *291*, 2400.
(25) Lasaga, A. C.; Luttge, A. *Am. Mineral.* **2004**, *89*, 527.
(26) Tang, R. K.; Orme, C. A.; Nancollas, G. H. *ChemPhysChem* **2004**, *5*, 688.
(27) Arvidson, R. S.; Davis, K. J.; Luttge, A. *Geochim. Cosmochim. Acta* **2005**, *69*, A779.
(28) Lasaga, A. C.; Luttge, A. *J. Phys. Chem. B* **2005**, *109*, 1635.
(29) Luttge, A. *Am. Mineral.* **2005**, *90*, 1776.
(30) Yanina, S. V.; Rosso, K. M.; Meakin, P. *Geochim. Cosmochim. Acta* **2006**, *70*, 1113.
(31) Meakin, P.; Rosso, K. M. *J. Chem. Phys.* **2008**, *129*, 204106.
(32) Zhang, L.; Luttge, A. *J. Phys. Chem. B* **2008**, *112*, 1736.
(33) Pizio, O.; Henderson, D.; Sokolowski, S. *J. Phys. Chem.* **1995**, *99*, 2408.
(34) Segura, C. J.; Chapman, W. G. *Mol. Phys.* **1995**, *86*, 415.
(35) Muller, E. A.; Rull, L. F.; Vega, L. F.; Gubbins, K. E. *J. Phys. Chem.* **1996**, *100*, 1189.
(36) Turner, C. H.; Johnson, J. K.; Gubbins, K. E. *J. Chem. Phys.* **2001**, *114*, 1851.
(37) Turner, C. H.; Pikunic, J.; Gubbins, K. E. *Mol. Phys.* **2001**, *99*, 1991.
(38) Hansen, N.; Jakobtorweihen, S.; Keil, F. J. *J. Chem. Phys.* **2005**, *122*, 11.
(39) Puibasset, J.; Pellenq, R. J. M. *J. Phys. Chem. B* **2008**, *112*, 6390.
(40) Nangia, S.; Garrison, B. J. *J. Am. Chem. Soc.* **2009**, *131*, 9538.
(41) Sariban, A.; Binder, K. *Macromolecules* **1988**, *21*, 711.
(42) Lyubartsev, A. P.; Martsinovski, A. A.; Shevkunov, S. V.; Vorontsovvelyaminov, P. N. *J. Chem. Phys.* **1992**, *96*, 1776.
(43) Panagiotopoulos, A. Z. *Mol. Simul.* **1992**, *9*, 1.
(44) Hao, M. H.; Scheraga, H. A. *J. Phys. Chem.* **1994**, *98*, 4940.
(45) Vasquez, M.; Nemethy, G.; Scheraga, H. A. *Chem. Rev.* **1994**, *94*, 2183.
(46) Dellago, C.; Bolhuis, P. G.; Csajka, F. S.; Chandler, D. *J. Chem. Phys.* **1998**, *108*, 1964.
(47) Accelrys Inc., *Cerius^2 Modeling Environment, Release 4.0*; Accelrys Inc.: San Diego, 1999.
(48) Feuston, B. P.; Garofalini, S. H. *J. Phys. Chem.* **1990**, *94*, 5351.
(49) Stillinger, F. H.; Rahman, A. *J. Chem. Phys.* **1978**, *68*, 66.
(50) Stillinger, F. H.; Weber, T. A. *Phys. Rev. B* **1985**, *31*, 5262.
(51) Feuston, B. P.; Garofalini, S. H. *Chem. Phys. Lett.* **1990**, *170*, 264.
(52) Blonski, S.; Garofalini, S. H. *Surf. Sci.* **1993**, *295*, 263.
(53) Garofalini, S. H.; Martin, G. *J. Phys. Chem.* **1994**, *98*, 1311.
(54) Martin, G.; Garofalini, S. H. *J. Non-Cryst. Solids* **1994**, *171*, 68.
(55) Martin, G.; Garofalini, S. H. *J. Phys. Chem.* **1994**, *98*, 1311.
(56) Litton, D. A.; Garofalini, S. H. *J. Appl. Phys.* **2001**, *89*, 6013.

JP909878B